An Exceptional Electron-rich Heteroaromatic Pentacycle for Ultralow Band Gap Conjugated Polymers and Photothermal Therapy

Christopher L. Anderson,[a,d] Tong Zhang,[b] Miao Qi,[a] Ziman Chen,[a,b] Chongqing Yang,[a] Simon J. Teat,[c] Nicholas S. Settineri,[c,d] Eric A. Dailing,[a] Andrés Garzón-Ruiz,[e] Amparo Navarro,[f] Yongqin Lv,[b] and Yi Liu*[a]*

[a]The Molecular Foundry, Lawrence Berkeley National Laboratory, Berkeley, California 94720, United States

[b]State Key Laboratory of Organic-Inorganic Composites, Beijing Key Laboratory of Bioprocess, Beijing University of Chemical Technology, Beijing, 100029, China

[c]Advanced Light Source, Lawrence Berkeley National Laboratory, Berkeley, California 94720, United States

[d]Department of Chemistry, University of California, Berkeley, California 94720, United States

[e]Department of Physical Chemistry, Faculty of Pharmacy, Universidad de Castilla-La Mancha, Cronista Francisco Ballesteros Gómez, Albacete 02071, Spain

[f]Department of Physical and Analytical Chemistry, Faculty of Experimental Sciences, Universidad de Jaén, Campus Las Lagunillas, Jaén 23071, Spain

KEYWORDS. conjugated polymers, electron donors, low band gap, near infrared, photothermal effect

ABSTRACT: Stable redox-active conjugated molecules with exceptional electron donating abilities are key components for the design and synthesis of ultralow band gap conjugated polymers. While hallmark electron rich examples such as pentacene derivatives have been thoroughly explored, their poor air stability has hampered their broad incorporation into conjugated polymers for practical applications. Herein, we describe the synthesis of the electron-rich, fused pentacyclic pyrazino[2,3-*b*:5,6-*b'*]diindolizine (PDIz) motif, and detail its optical and redox behavior. The PDIz ring system exhibits a lower oxidation potential and reduced optical band gap than the isoelectronic pentacene while retaining greater air stability in both solution and the solid state. The enhanced stability and electron density, together with

readily installed solubilizing groups and polymerization handles, allow for the use of the PDIz motif in the synthesis of a series of conjugated polymers with band gaps as small as 0.71 eV. The tunable absorbance throughout the biologically-relevant near infrared I and II regions enables the use of these PDIz-based polymers as efficient photothermal therapeutic reagents for laser ablation of cancer cells.

INTRODUCTION

Small band gap conjugated polymers that absorb low-energy visible and near infrared (NIR) light have attracted great attention for their applications in photovoltaics, photodetectors, light emitting diodes and bioimaging.[1-3] Recently, small band gap polymers have emerged as a viable candidate for noninvasive photothermal therapy (PTT) due to their ability to induce cell apoptosis or necrosis by converting absorbed photon energy in the biologically-relevant NIR regions into heat.[4-7] While early stage PTT research is mainly focused on using light sources in the first NIR window (NIR-I, 750–1000 nm), significant emerging interest has been devoted to the utilization of the so-called NIR-II region in the range of 1000–1700 nm, due to its increased tissue penetration, less endogenous absorption and scattering, and higher maximum permissible exposure.[8-10]

In addition to the absorption prerequisite, the polymers available for use as PTT active agents are winnowed further by the requirement that they must efficiently convert light into heat, which requires that they have few radiative relaxation pathways and thus are not highly fluorescent.[6] Donor-acceptor polymers,[11] which contain covalently-linked alternating electron donating (donor) and electron withdrawing (acceptor) units in the polymer backbone, are specifically suited for PTT on account of their modularly tunable optical properties and their intrinsic non-radiative deexcitation through intramolecular charge-transfer. The optical properties of these polymers are strongly related to the electronic band gap (E_g), defined by the highest occupied molecular orbital (HOMO) energy levels and the lowest unoccupied molecular orbital (LUMO) energy levels,[2] which are dominated by the electronic properties of the donor and acceptor repeat units, respectively, through frontier orbital hybridization. Judiciously chosen electron donor and acceptor pairs are deterministic to the polymer's optical and electrical band gaps. In order to produce polymers with NIR absorbances—especially NIR-II absorbances—very strong donor and acceptor monomeric building blocks are desired.

In the effort to create tailor-made small band gap polymers, great strides have been made, mostly through the development of potent electron acceptors, such as benzobisthiadiazole (BBT),[12] diketopyrrolopyrrole (DPP),[13-19] and nathphalenediimide (NDI).[20-26] In contrast, less attention has been paid to the development of practical strongly electron rich donors with high lying HOMO levels. The majority of the electron donors employed in low band polymers are thiophene derivatives, the electron affinity of which can be further improved by cross conjugation[27] or more commonly, by extending the π-system through annulation.[28-29] Linear acenes are another representative class of non-thiophene-based electron-donating systems with hallmark optoelectronic properties.[30] As the number of linearly fused rings increases in linear fused acenes, the HOMO level is raised significantly together with a reduced HOMO-LUMO gap.[31] However, this molecular orbital modulation also leads to significantly decreased air and chemical stability, limiting the use of pentacene and longer fused acenes as electron rich repeat units in conjugated polymers.[32-33]

One common approach to stabilize linear acenes is to incorporate heteroatoms like nitrogen into the aromatic skeleton. Introducing pyridyl nitrogen atoms, however, leads to decreased electron density and thus lowers HOMO level, such as those observed in azaacenes.[34-36] When nitrogen atoms are substituted at bridgehead positions, like those in indolizine rings,[37] electron donating character can instead be engendered due to the full participation of the nitrogen lone pair in the ring. Incorporating indolizines into extended pentacyclic π-systems such as benzodiindolizine (BDI, Scheme 1a) gives rise to a small band gap, electron-rich chromophore that exhibits HOMO-LUMO characteristics comparable to the structurally analogous TIPS-pentacene.[38] Nevertheless, the atmospheric stability of these compounds in solution is less than satisfactory despite the installation of two silylethynyl groups on the reactive central benzene ring, and the utility of such aromatic units in conjugated polymers is lacking.

Herein, we devised a pyrazino[2,3-*b*:5,6-*b'*]diindolizine (PDIz) system where the most reactive carbons of the BDI skeleton are replaced by pyrazyl nitrogen atoms, which significantly improved the air stability despite an even higher-lying HOMO level and a further decreased HOMO-LUMO gap. Through a unique rearrangement of an ionic *para*-azaquinodimethane (iAQM) ring system,[39] this class of redox-active pentacycles can be generated with facile incorporation of solubilizing groups and reactive coupling groups for polymerization. The redox-active PDIz motif displays both electron-rich character of its two indolizine ring systems and the electron-deficiency of the central pyrazine ring, while

retaining excellent stability. When copolymerized with electron acceptor building blocks, the extraordinary electron donating character of the PDIz ring system imbues these conjugated polymers with high lying HOMO levels and notably small optical band gaps as low as 0.7 eV. Several of these polymers showed notable performance as active agents in both NIR-I and NIR-II photothermal therapy.

RESULTS AND DISCUSSION

Materials Synthesis. The construction of the pentacyclic PDIz core was built atop the unprecedented reactivity of the recently discovered quinoidal AQM unit.[40-42] AQM ditriflates, such as **3a**, could be obtained in two steps from 1,4-diacetyl-2,5-diketopiperazine (**1**) (Scheme 1b).[43] When those AQM ditriflates were heated in solution in the presence of pyridine or one of its derivatives, nucleophilic displacement reactions were expected.[39] In contrast to the previously reported thiophenylidine-flanked AQM ditriflates, the bispyridinium displacement products of diphenylidine AQM ditriflates were not isolated, instead a spontaneous intramolecular cyclization occurred to produce substituted pyrazino[2,3-*b*]indolizines such as **4a** in high yields. It was then postulated that the pentacyclic PDIz motif would be accessible via a base-promoted intramolecular cyclization and subsequent dehydrogenation on the remaining pyridinium unit (see Scheme S3 in SI). Indeed, under appropriate basic reaction conditions, this cascade of reactions yields the symmetrical, annulated, pentacyclic **PDIz:OC6**. Other PDIz derivatives could be obtained following similar reaction protocols (Schemes 1c and S1). When both of the hexyloxy groups in PDIz:OC6 were replaced with hydrogen, the corresponding **PDIz:H** could be obtained, which showed appreciable but limited solubility in common organic solvents. It appears that the appendage of two hexyloxy groups to the phenyl end groups increases both the solubility and the yield of **PDIz**. Substituted pyridine precursors, such as 4-thienyl- and 4-$(Bu)_3$Sn-pyridine, were also employed to give PDIz derivatives such as **Th-PDIz:C6** and **Sn-PDIz:C12** (Scheme 1c), respectively, which displayed substantial effects in their optical band gaps (see discussions later). The successful incorporation of the stannyl end groups is essential for the incorporation of the **PDIz** unit into the backbone of conjugated polymers. Other solubilizing groups, such as dodecyloxy and tetraethylene glycol methyl ether were attached to the phenyl side groups to engender high solubility and to affect different hydrophilicity in **Sn-PDIz:C12** and **Sn-PDIz:O4EG**, respectively (Scheme 1c). Polymerization of those PDIz monomers

with properly chosen aryl dibromide co-monomers via Stille polycondensation would give rise to novel conjugated polymers with desirable optoelectronic properties. A variety of aryl dibromide co-monomers, including the electron accepting BBT, DPP and NDI derivatives, were employed in the copolymerization of **Sn-PDIz:C12** to give **P1**, **P3**, and **P4**, respectively. The copolymerization of BBT as well as the electron rich thiophene dibromide, with **Sn-PDIz:O4EG** afforded **P2** and **P5**, respectively bearing the more hydrophilic tetraethylene glycol methyl ether side chains (Schemes 2 and S2). Polymers **P1**–**P5** have number-averaged molecular weights (Mn) in the range of ~ 0.5×10^4 to ~1.4×10^4 Daltons by size-exclusion chromatography (SEC) (Figure S18). The successful synthesis of **P1-P5** demonstrated the synthetic versality of a larger array of **PDIz** polymers with widely varying electronic structures and side-chain polarities.

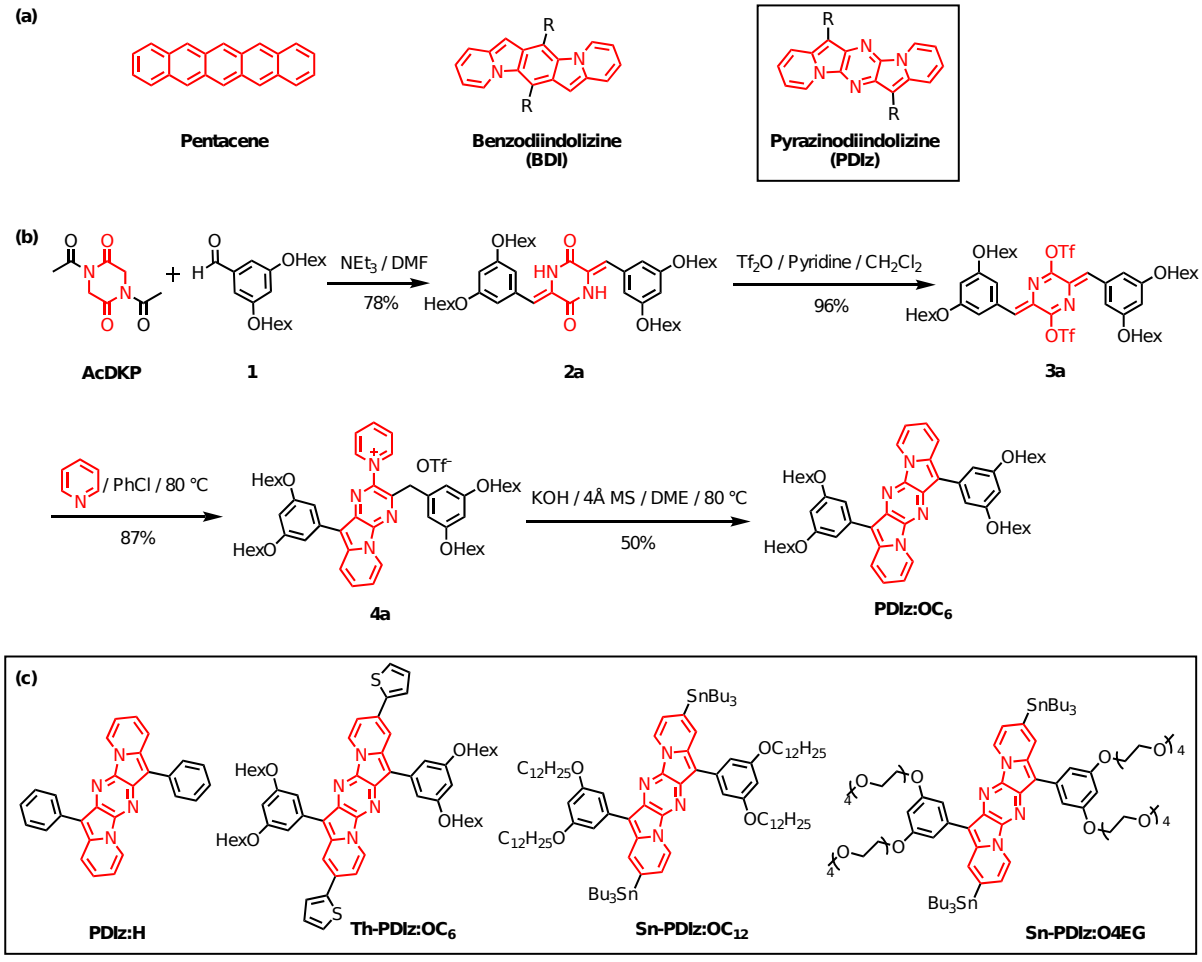

Scheme 1. (a) Exemplary electron-rich pentacyclic conjugated ring systems. (b) The synthesis of **PDIz:OC$_6$** (DMF: *N*,*N*-dimethylformamide, Tf_2O: trifluoromethanesulfonic anhydride, PhCl: chlorobenzene, 4Å MS: 4Å molecular sieves, DME: 1,2-dimethyoxyethane). (c) A series of PDIz derivatives synthesized in an analogous fashion.

Scheme 2. The synthesis of low band gap polymers **P1**-**P5** via the polymerization of PDIz-based monomers with various aryl dibromides.

X-ray Crystallography. **PDIz:H**, **PDIz:OC$_6$**, and **Th-PDIz:OC$_6$** were characterized by single crystal X-ray crystallography and the structures are summarized in Figures 1 and S9-S11. In the solid state, all three PDIz compounds exhibit planar fused pentacyclic cores with their two appended phenyl rings tilted out of plane by 35°–40°. **PDIz:H** and **Th-PDIz:OC$_6$** both pack in slip-stacked columns wherein there is significant π-overlap between adjacent molecules without translation along the short-axis of each fused system and each pentacyclic plane rests ~3.4 Å from its neighbors (Figures 1d, 1f, S10, and S12). Additionally, in the solid-state structure of **Th-PDIz:OC$_6$**, the appended thiophene rings sit in plane with the PDIz pentacycle. In contrast to the other two PDIz molecules, **PDIz:OC$_6$** packs in trimeric stacks, with the fused pentacyclic core on each molecule insulated from the cores of its neighbors by their bis(hexyloxy)phenyl groups (Figures 1e and S11), indicating the high dependency of the solid state packing behavior on the substituents. In addition, **Sn-PDIz:O4EG** was crystallized in the presence of KPF_6. Despite the low-resolution of its X-ray structure, it was adequate to confirm the integrity of the structure and coordination of potassium ions by the side-chains (Figure S13). The single crystal structure of the monocyclized intermediate **4a** as a PF_6^- salt was also obtained (Figure S4). Intriguingly, the solid-state packing of intermediate **4a** is highly anisotropic, forming trimeric aggregates which further assemble into helical columns.

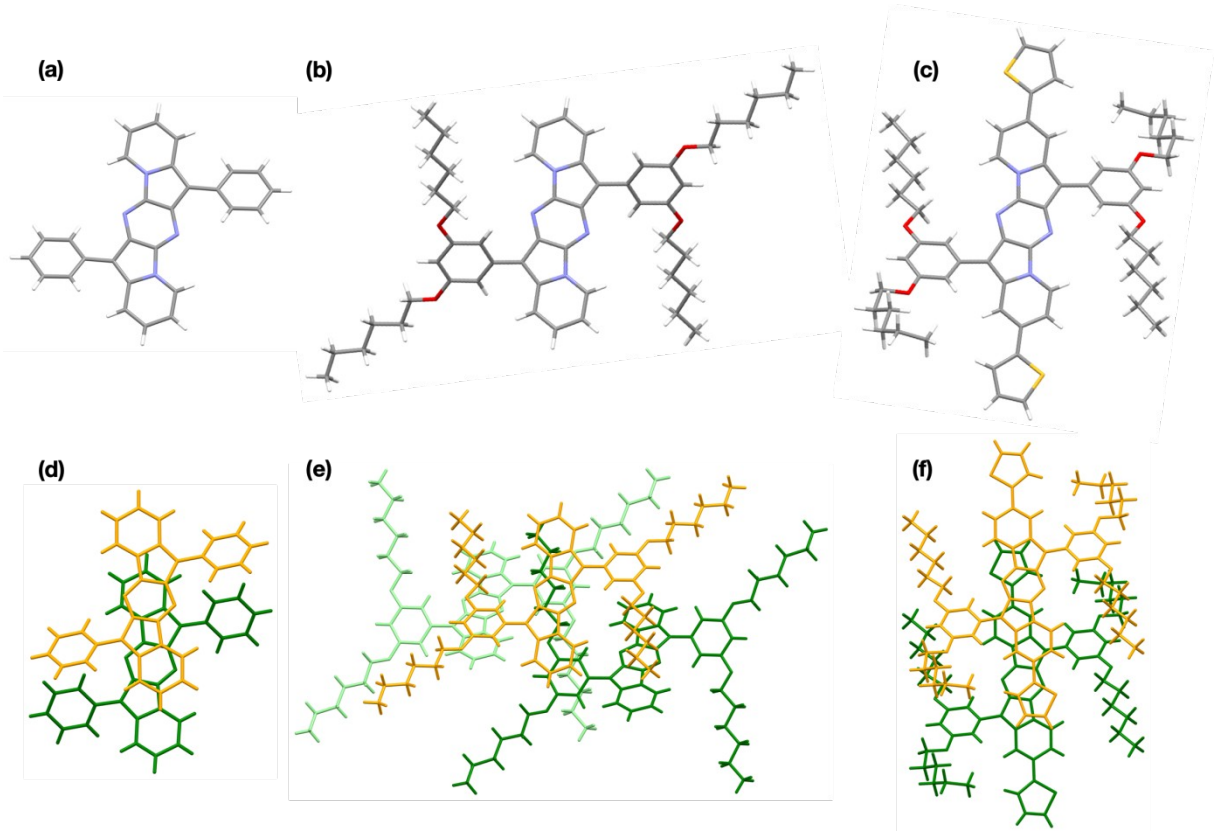

Figure 1. Single crystal X-ray structures of (a) **PDIz:H**, (b) **PDIz:OC$_6$** and (c) **Th-PDIz:OC$_6$** (carbon = gray, hydrogen = white, oxygen = red, nitrogen = blue, sulfur = yellow). Solid-state packing of (d) **PDIz:H**, (e) **PDIz:OC$_6$** and (f) **Th-PDIz:OC$_6$** (front = orange, middle = lime green, back = forest green).

Optical and Redox Properties of PDIz Small Molecules and Polymers. PDIz:H displays an intense blue color in both the solid state and in solution, hinting at its notably small optical gap. Its UV-Vis spectrum shows an absorption maximum and edge at 650 nm and 674 nm (Figure 2), respectively, which is shifted bathochromically compared to the isoelectronic pentacene and benzoannulated BDI.[38] The UV-Vis spectra of **PDIz:H**, **PDIz:OC$_6$**, **Th-PDIz:OC$_6$**, **Sn-PDIz:OC$_{12}$** and **Sn-PDIz:O4EG** all show four sub-peaks, corresponding to the so-called "p-bands" pattern[44] that is also observed in the spectra of BDI and pentacene derivatives. The hexyloxyl substituents on the phenyl groups have a minimal impact on the absorption properties of the PDIz core. On the other hand, the appendage of $SnBu_3$ and thiophene groups on the PDIz skeleton induces significant red shifts (~20 nm and 50 nm, respectively), suggesting a more effective electronic tuning in this conjugation pattern (Figure 2, Table 1).[30] **PDIz:H** has a low quantum yield of 1.6%. Other PDIz derivatives are also

weakly fluorescent. The fluorescence spectroscopy of **PDIz:H** shows two peaks, with the lower wavelength peak yielding a small Stokes shift of 30 nm (Figure S3), in accordance with aromatic systems with rigid and planar structures.

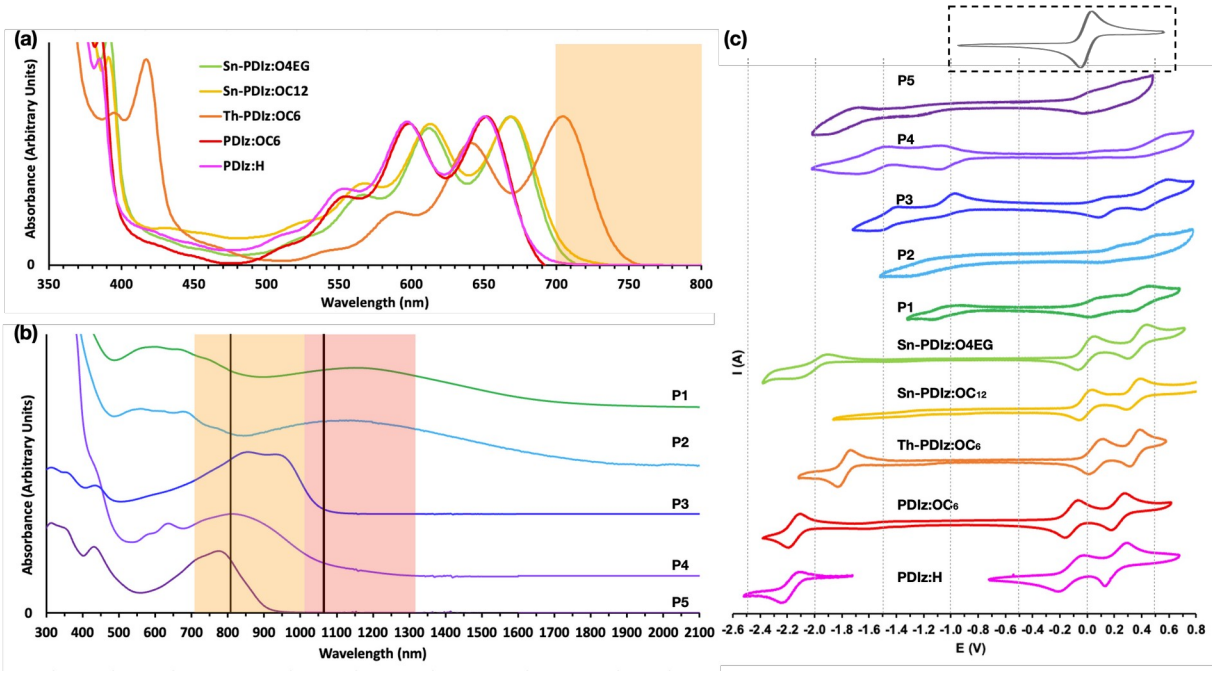

Figure 2. Optical and electrochemical properties of PDIz small molecules and polymers. (a) UV-Vis-NIR spectra of PDIz small molecules (in CH_2Cl_2 solution). The NIR-I window is highlighted in orange. (b) UV-Vis-NIR spectra of polymers **P1**-**P5** (in CCl_4 solution), with the NIR-I window highlighted in orange and the NIR-II window in red. Additionally, the common laser wavelengths accessing these two windows that are used in PTT are shown as black lines at 808 and 1064 nm. (c) CV traces of PDIz small molecules and polymers **P1**-**P5** (CH_2Cl_2, 100 mM NBu_4PF_6, 100 mV/s, vs. Fc/Fc^+). Inset is the CV of Fc/Fc^+, which was used as the external standard. Note: CV of **PDIz:H** was acquired in two separate scans due to deposition of redox product on electrodes. Currents are scaled arbitrarily to allow for comparison between traces.

Cyclic voltammetry (CV) of **PDIz:H** and its derivatives each display two electrochemically-reversible oxidation waves at remarkably low onset potentials, along with one reversible reduction wave (Figure 2c). The $E_{1/2}$ value for the first oxidation wave of **PDIz:H** falls below that of the ferrocene/ferrocenium (Fc/Fc^+) redox pair, a commonly used electrochemical reference. An electrochemical E_{HOMO} level of -4.6 eV was derived from the electrochemical responses of **PDIz:H**, indicating that the PDIz motif is highly electron rich.

The reversible reductive peak observed in the CV of **PDIz:H** corresponds to an $E_{1/2}^{red}$ of around -1.55 V and an electrochemical HOMO-LUMO gap of 1.90 eV (Figure 2c and Table 1). The electrochemical gaps of these PDIz derivatives are in good agreement with the observed optical gaps (Table 1). Compared to the BDI pentacycle (E_{HOMO} = -4.83 eV), **PDIz:H** is even more electron rich (E_{HOMO} = -4.65 eV) and has narrower optical and electrochemical gaps despite the incorporation of the electron-deficient Pyrazine unit (see discussions later).

Table 1. A summary of the frontier orbital energy levels and band gaps of the PDIz small molecules and polymers obtained from optical, electrochemical, and computational characterization. Lowest-energy transition wavelengths (λ_{vert}^{calc}) and oscillator strengths (*f*) for the $S_0 \rightarrow S_1$ electronic transition calculated at the PBE0/6-31+G** level of theory (lanl2dz in the case of Sn compound) in CH_2Cl_2 solution.

Compound	Optical				Electrochemical[a]				Theoretical[d,e]					
	λ_{max} (nm[eV])	ε (L mol^{-1} cm^{-1})	λ_{onset} (nm)	E_g^{Opt} (eV)	E_{red} (V)	E_{ox} (V)	HOMO (eV)	LUMO (eV)	E_g^{CV} (eV)	HOMO (eV)	LUMO (eV)	E_g^{calc} (eV)	λ_{vert}^{calc} (nm[eV])	*f*
PDIz:H	651[1.90]	6501.7	674	1.84	-2.05	-0.15	-4.65	-2.75	1.90	-5.09	-2.41	2.68	613[2.02]	0.16
PDIz:OC$_6$	652[1.90]	6022.2	674	1.84	-2.07	-0.20	-4.60	-2.73	1.87	-5.10	-2.41	2.69	613[2.02]	0.16
Th-PDIz:OC$_6$	704[1.76]	20110.9	741	1.67	-1.70	-0.04	-4.76	-3.10	1.66	-5.03	-2.62	2.41	677[1.83]	0.51
Sn-PDIz:OC$_{12}$	669[1.85]	12276.4	704	1.76	—[f]	-0.08	-4.72	—[f]		-5.10	-2.42	2.68	604[2.05]	0.24
Sn-PDIz:O4EG	668[1.86]	—[g]	702	1.77	-1.93	-0.08	-4.72	-2.87	1.85	—[c]	—[c]	—[c]	—[c]	—[c]
P1	1146[1.08]	10358.6[b]	1740	0.71	-0.86	-0.08	-4.72	-3.94	0.78	—[c]	—[c]	0.67[h]	—[c]	—[c]
P2	1140[1.09]	23497.1 [b]	1795	0.69	-0.81	0.08	-4.88	-3.99	0.89	—[c]	—[c]	—[c]	—[c]	—[c]
P3	772[1.61]	17129.3[b]	915	1.36	-0.89	0.00	-4.80	-3.91	0.89	—[c]	—[c]	—[c]	—[c]	—[c]
P4	813[1.53]	35624.6 [b]	1090	1.14	-0.84	0.00	-4.80	-3.96	0.84	—[c]	—[c]	—[c]	—[c]	—[c]
P5	856[1.45]	27259.7[b]	1050	1.18	-1.02	-0.12	-4.68	-3.78	0.9	—[c]	—[c]	—[c]	—[c]	—[c]

[a] referenced to Fc/Fc^+. [b] polymer extinction coefficients are assuming infinite chains. [c] not calculated. [d] side-chains truncated as methoxy groups where applicable. [e] PBE0/6-31+G** (lanl2dz in the case of Sn compound). [f] not observed. [g] not measured. [h] PBE0/6-31G*.

Due to the exceptionally electron rich nature of the PDIz core, its stable oxidative states can be readily reached by chemical oxidation. Mixing **PDIz:H** in stoichiometric amounts with a number of chemical oxidants such as iron (III) chloride ($FeCl_3$), Tris(4-bromophenyl)ammoniumyl hexachloroantimonate (magic blue), 2,3-dicyano-5,6-dichloroquinone (DDQ) or 2,3,5,6-tetrafluoro-tetracyanoquinodimethane (F_4TCNQ) produces chartreuse solutions. UV-Vis-NIR spectroscopy revealed that the main absorption features of the products are nearly identical to each other with multiple absorption features between 700 nm and 1400 nm, indicative of the formation of the radical cation **PDIz:H**$^{\bullet+}$ (Figure 3b). Infrared spectroscopy revealed spectroscopic changes that were consistent with the formation of oxidated products (Figure S14). Spectroelectrochemical studies of **PDIz:OC$_6$** showed electrochemical oxidation-induced spectroscopic changes throughout two potential windows, corresponding to the stepwise 2-electron oxidation of the PDIz core. As shown in Figures 3c and d, new absorption features in the 700-1000 nm window emerged as the oxidation potential was raised from -0.45 V to 0.45 V (vs. Fc/Fc^+), which were similar to the absorption spectra of the chemically-oxidized **PDIz:H**$^{\bullet+}$ and confirmed the formation of the radical cation **PDIz:OC$_6$**$^{\bullet+}$. Further increase in the potential led to the disappearance of the PDIz radical cation absorption peaks, with the concomitant appearance of two broad peaks at 490 nm and 740 nm that were ascribed to the formation of **PDIz:OC$_6$**$^{2+}$. The spectroelectrochemical process was fully reversible, evidenced by the full recovery of the absorption of the neutral **PDIz:OC$_6$** upon a reversed potential scan (Figure S15).

Despite the low oxidation potential of **PDIz:H** and its derivatives, these compounds displayed high stability towards atmospheric oxygen in both the solid state and solution, in sharp contrast to most other pentacene derivatives. As shown in Figure S16, repeated sparging of the solution of **PDIz:H** with compressed air over the course of months slowly resulted in spectroscopic changes, indicating that there was a very slow oxidation reaction between the solution of **PDIz:H** and atmospheric oxygen.

The PDIz-based polymers **P1-P5** show significantly reduced optical and electrochemical band gaps with respect to their PDIz monomers, as revealed by UV-Vis-NIR and CV studies (Figures 2b and 2c, Table 1). Among those polymers, the donor-donor polymer **P5** has the largest optical band gap at 1.36 eV, while all the other donor-acceptor polymers have an absorption edge beyond 1000 nm. Polymers **P3** and **P4** have substantial absorptions in the NIR-I window, and, very notably, both **P1** and **P2** have a broad absorption

across the NIR-II region. These absorption spectra correspond to optical band gaps as low as 0.71 eV and electrochemical band gaps around 0.78 eV (Figure 2b, Table 1). While the HOMO levels of **P1** and **P2** are close to those observed in the PDIz small molecules, their LUMO levels are significantly lowered due to the presence of the strongly electron-withdrawing BBT unit. In addition, the polymers have shown excellent air stability, as revealed by their solution UV-Vis-NIR spectra that remained nearly identical after 12 hrs (Figure S17).

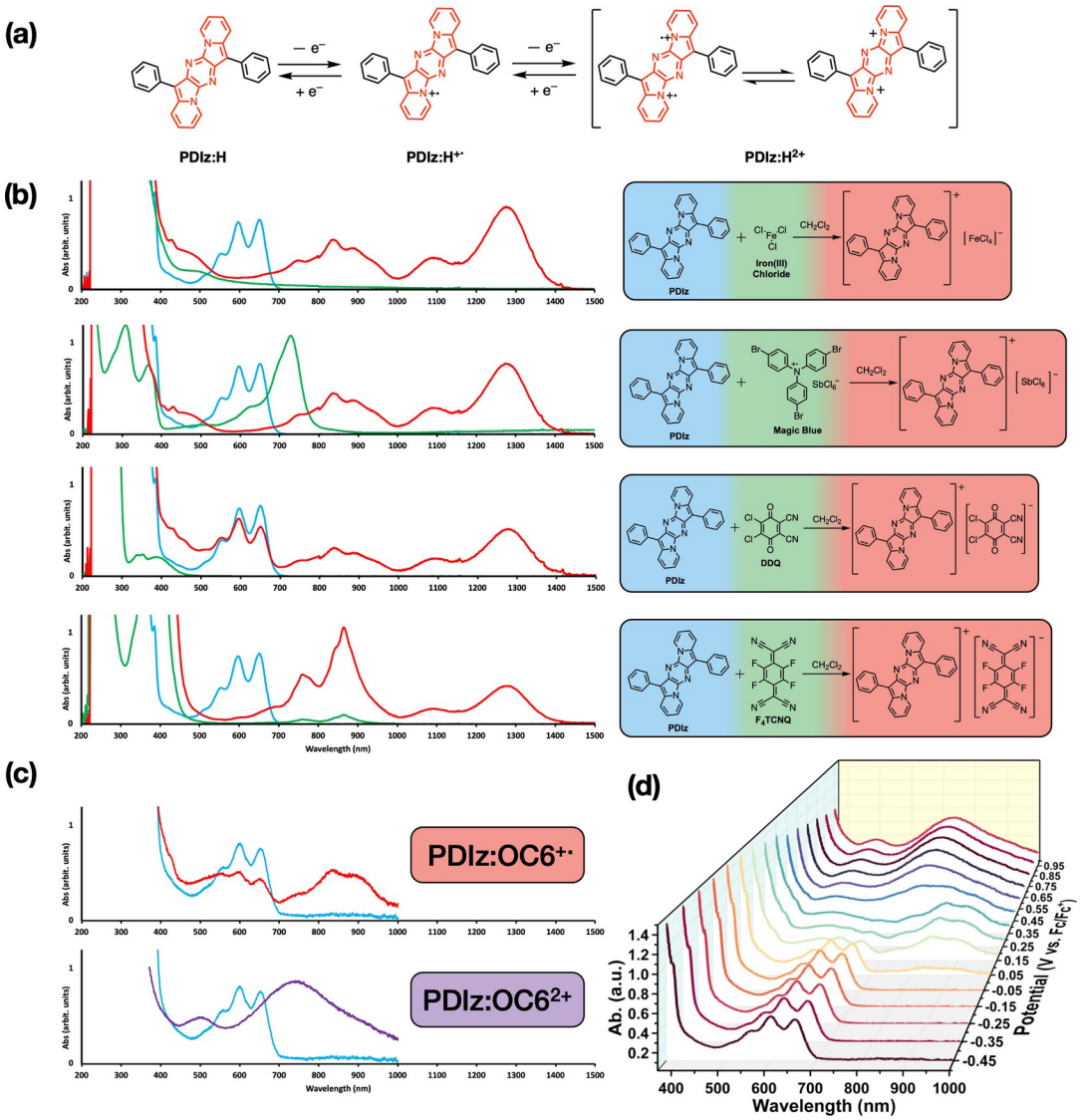

Figure 3. (a) Schematics showing the stepwise oxidation reactions of **PDIz:H**. (b) UV-Vis-NIR traces of the one-electron oxidation reaction between **PDIz:H** (sky blue) and various electron acceptors (green) to produce **PDIz:H**$^{\bullet+}$ (red). (c) Overlay of UV-Vis spectra of the neutral **PDIz:OC$_6$** with its radical cation (top, obtained at +0.15 V vs. Fc/Fc$^+$) and dication

(bottom, obtained at +0.95 V vs. Fc/Fc^+), respectively, according to (d) the spectroelectrochemical traces within the potential windows between -0.45 V and 0.95 V.

Theoretical Modelling. The molecular structure and electronic properties of **PDIz:H** and its derivatives **PDIz:OC$_6$**, **Th-PDIz:OC$_6$** and **Sn-PDIz:OC$_{12}$** were computationally explored at the PBE0/6-31+G** level in CH_2Cl_2 solution (Figure 4). The geometric optimization of **PDIz:H** mirrored its X-ray structure in producing a somewhat contorted central pyrazine ring, with its ring nitrogen atoms adopting internal angles of 112° (the analogous angle is 111.16° in the X-ray structure). The appended phenyl substituents are twisted (38º) with respect to the plane of the pentacycle, in concordance with the X-ray structure. The phenyl substituents are also twisted for **PDIz:OC$_6$**, **Th-PDIz:OC$_6$** and, to a lesser degree, for **Sn-PDIz:OC$_{12}$**. The frontier molecular orbital (FMO) diagrams of **PDIz:H** show that electronic density is well spread across the fused pentacycle core, in accordance with the high delocalization of π electrons in extended conjugated systems (Figure S1a). The presence of pyrazine nitrogen atoms in PDIz derivatives leads to a decrease of the HOMO energy and, in greater extent, of the LUMO energy, resulting in a band gap narrowing relative to the pentacyclic benzo-analog BDI (Figure S1b).[38] The phenyl substituents also have a contribution to the band gap narrowing as well as to the electron density of the HOMO. Thus, the presence of pyrazine nitrogen atoms and phenyl rings lead to a narrower band gap for **PDIz:H** than for the BDI derivative.[38] In the HOMO orbital density diagram, there is a node on the 3- and 5- positions of each phenyl group, indicating that substitution at these positions has little impact on the electronics of the PDIz system.

The lowest-energy transition wavelengths (λ_{vert}^{calc}) calculated for **PDIz:H** and its derivatives in CH_2Cl_2 solution match well with the absorption maxima collected in Table 1 (differences in energy $\leq$ 0.20 eV). All of them correspond to $S_0 \rightarrow S_1$ electronic transitions involving HOMO and LUMO molecular orbitals with 99% contribution. The small band gap polymer, **P1**, was also modeled using periodic boundary conditions (PBC) at the PBE0/6-31G* level. A theoretical band gap of 0.67 eV was predicted for an infinite single chain of **P1**, which closely matched the optical and electrochemical results described above. Non-coplanarity arose from steric crowding between the BBT unit and the neighboring PDIz units (Figure 4c and S4), as indicated by a tilt angle of 26°. The presence of such a twist may be responsible for widening the band gap of the resulting polymer, without which an even

smaller gap is expected based on the frontier molecular orbital levels of the chosen donor-acceptor pair.

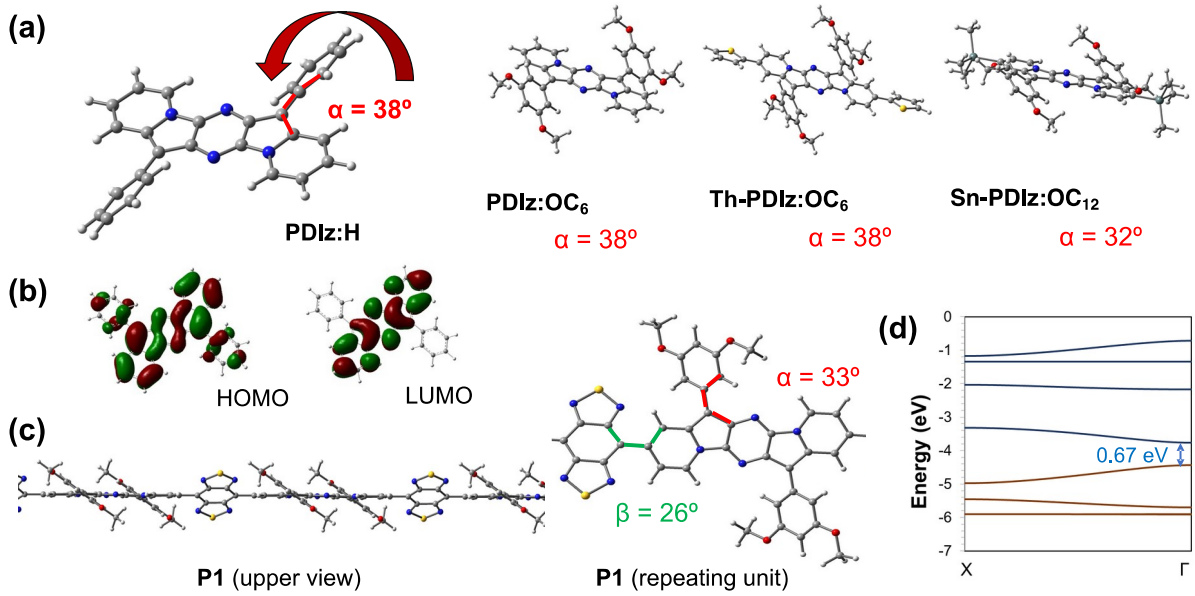

Figure 4. (a) Molecular structures computed for **PDIz:H**, **PDIz:OC$_6$**, **Th-PDIz:OC$_6$**, **Sn-PDIz:OC$_{12}$** at the PBE0/6-31+G** level of theory in CH_2Cl_2 solution (α is the dihedral angle between the side phenyl rings and the pentacyclic plane; alkyl side chains were truncated to methoxy groups but the names **PDIz:OC$_6$**, **Th-PDIz:OC$_6$**, **Sn-PDIz:OC$_{12}$** have been maintained to avoid confusion). (b) HOMO and LUMO orbital density diagrams of **PDIz:H** (isocontour plots 0.02 a.u.). (c) The optimized geometry of an infinite chain of **P1** at the PBE0/6-31G* level of theory using PBC. The upper view shows steric effects pushing the PDIz and BBT monomers out of plane from each other (β is the dihedral angle between PDIz and BBT moieties). (d) Electronic band structures calculated for an isolated periodic chain of **P1** at the PBE0/6-31G* level of theory. The high symmetry *k*-points are Γ(0.0, 0.0, 0.0) and X(0.5, 0.0, 0.0) in reciprocal space coordinates.

Photothermal Effects of PDIz Polymers. The remarkable NIR absorption properties of the PDIz polymers prompted us to evaluate the potential of **P3** and **P4** as NIR-I PTT active materials and **P2** as a NIR-II PTT active material. When a THF solution of **P2** (100 μg/mL) was exposed to a 1064 nm laser under 1.5 W cm^{-2}, a maximum temperature change (ΔT_{max}) of 32.8 ºC was observed after 5 min (Figure 5a). Likewise, both polymers **P3** and **P4** showed ΔT_{max} values of 36.7 ºC under the same conditions after irradiation by an 808 nm laser. In order to assist the dispersion of these relatively nonpolar polymers in water and facilitate their interactions with biological targets, a nanoprecipitation method was adopted to process them

into self-assembled polymer nanoparticles (PNPs) in the presence of the surfactant DSPE-mPEG2000.[45] The so-produced PNPs have hydrodynamic radii of 175.1 nm ± 6.2 (**P2**), 95.7 nm ± 1.0 (**P3**), and 149.9 nm ± 1.6 (**P4**) as revealed by dynamic light scattering (DLS) (Figure S19), which were also corroborated with scanning electron microscopic (SEM) results (Figure 5c-e). The loading efficiency, defined by Equation S1, reached above 73%, as revealed by UV-Vis studies (Table S1). Subsequent PTT studies revealed that the PNPs retained the photothermal conversion abilities of their parent polymers. For aqueous dispersions containing 100 μg/mL of the PNPs, ΔT_{max} values of ~30 ºC could be realized for the **P2**-PNPs irradiated at 1064 nm and **P3** and **P4**-PNPs irradiated at 808 nm at 1.5 W cm^{-2} for 5 min (Figures 5f and 5g). The temperature increase is also dependent on laser intensity (Figure S20). Photoconversion efficiencies (PCEs, η) of these PNPs were determined to be 28.3% (**P2**), 28.3% (**P3**), and 27.3% (**P4**), respectively (Figure S21 and Table S2), which is on par with or better than the conventional inorganic nanomaterials such as $Cu_{2-x}S$ nanocrystals (16.3%),[46] gold nanoshells (13%) and nanorods (21%), $Cu_{2-x}Se$ (22%)[47] and MoS_2 nanosheets (24.4%). The efficiencies are also comparable to existing semiconducting PNPs, such as poly(cyclopentadithiophene-alt-diketopyrrolopyrrole) NPs (20%),[48] heterocyclic conductive PPDS NPs (31.4%),[49] poly-2-phenyl-benzobisthiazole NPs (32.4%),[50] poly(silolodithiophene-alt-diketopyrrolopyrrole NPs (35%),[51] and amphiphilic hyperbranched polyporphyrins vesicles (44.1%).[52] While our PTT agents did not show the highest PCEs, the unoptimized results reported here have revealed the potential of this new class of polymers, especially for use as NIR-II absorbers. Furthermore, the heating and cooling cycles have been conducted consecutively 4 times in air for all the PNPs with no signs of efficiency deterioration, indicating that these PNPs have high stability towards the air, heat and photobleaching (Figure S22).

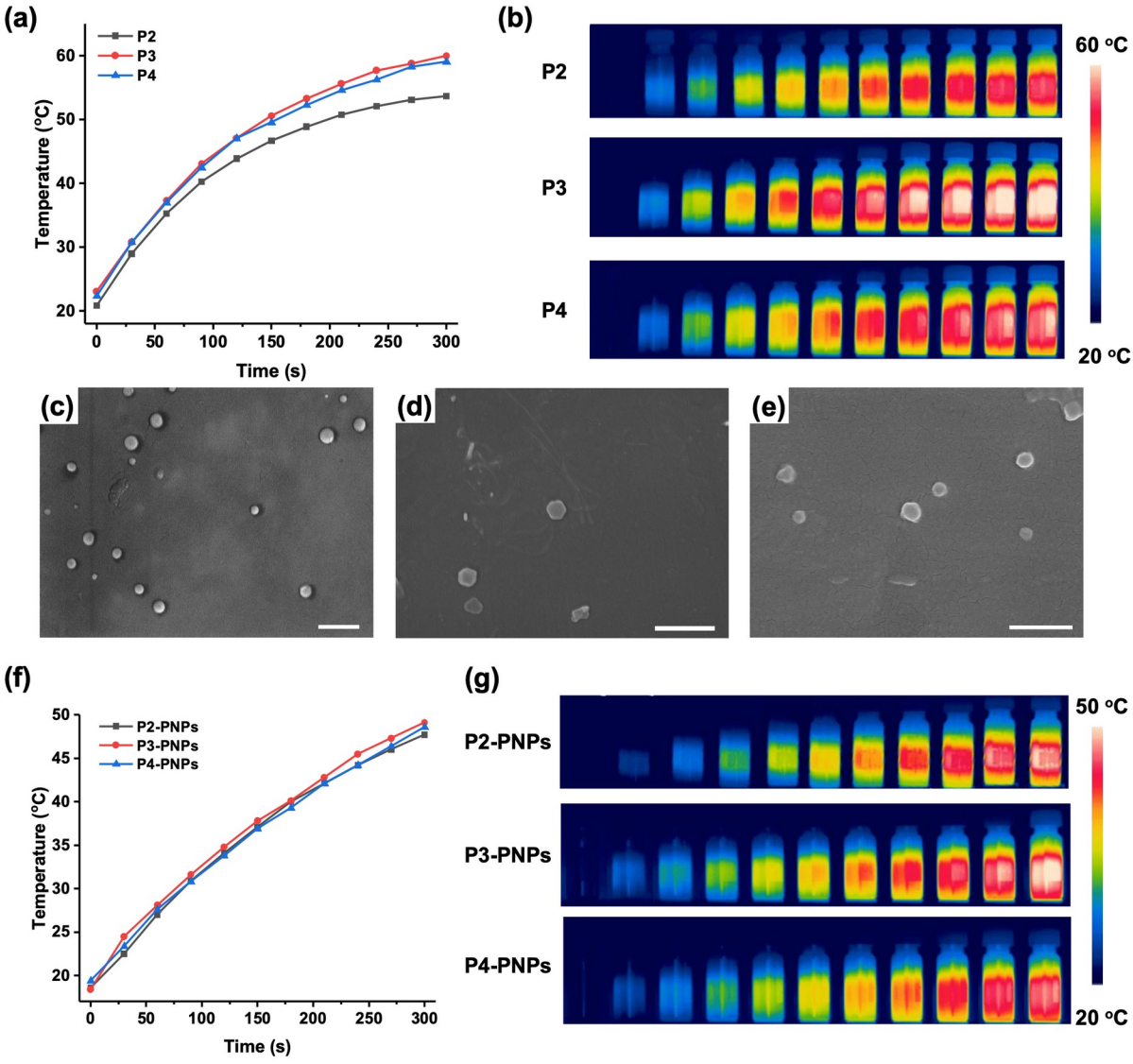
(a)
P2
P3
P4
Temperature (°C)
Time (s)
(b)
P2
P3
P4
60 °C
20 °C
(c)
(d)
(e)
(f)
P2-PNPs
P3-PNPs
P4-PNPs
Temperature (°C)
Time (s)
(g)
P2-PNPs
P3-PNPs
P4-PNPs
50 °C
20 °C

Figure 5. (a) Temperature variations of **P2**–**P4** solutions in THF (100 μg/mL) under 1064 nm (**P2**) or 808 nm (**P3** and **P4**) laser irradiation (1.5 W/cm^2) and (b) the corresponding IR images. SEM images of **P2**-PNPs (c), **P3-**PNPs (d) and **P4**-PNPs (e) (scale bar: 500 nm). (f) Temperature variations of aqueous **P2-P4** PNPs (0.5 mg/mL) under 1064 nm (**P2** PNPs) or 808 nm (**P3** PNPs and **P4** PNPs) laser irradiation (1.5 W/cm^2), and (g) the corresponding IR images.

Two cell lines—4T1 (mouse breast adenocarcinoma) and B16 (mouse melanoma cells) cells, were employed for in vitro evaluation of the PTT effects of **P2-P4** PNPs. As shown in Figures 6b-c and S20, both cell lines—after incubation with various amounts of **P3** and **P4** PNPs—maintained over 74% viability at a loading of 250 μg/mL without laser irradiation. After 3 min irradiation using an 808 nm laser at 1.5 W/cm^2, the cell viabilities dropped significantly, with the **P3**-PNPs and **P4**-PNPs treated cells dropping to 10% and 17% for 4T1, and 16% and 13% for B16 cells, respectively. The **P2**-based PNPs exhibited a lower latent cytotoxicity, giving cell viabilities of 94% and 90% at a loading of 250 μg/mL for 4T1 and B16 cells, respectively (Figure 6a and S23). When irradiated using a 1064 nm laser at 1.5 W/cm^2 for 3 min, cell viability dropped to 33% and 36% for 4T1 and B16 cells, respectively (Figure 6a and S23). The decreased cell viability corroborates well with the confocal laser scanning microscopy images showing significantly reduced numbers of living cells after irradiation (Figure 6d). Overall, the relatively low cytotoxicity and good photothermal performance of these PNPs in two different NIR windows demonstrate the great potential of PDIz-based narrow band gap polymers as a promising materials platform for photothermal therapy.

CONCLUSION

We have presented a facile synthetic method yielding the PDIz fused pentacyclic aromatic ring system, composed of two strongly electron donating indolizines and an electron-withdrawing pyrazine core. The PDIz motif behaves as an exceptionally electron rich building block that features a low oxidation potential and a small HOMO-LUMO gap. Additionally, it displays excellent air stability due to the presence of two pyrazine-type nitrogen atoms that block the normally reactive sites on pentacene derivatives. The facile synthesis of the PDIz motif can be readily used to introduce solubilizing groups and polymerization handles onto the PDIz core, allowing for its use as a super electron-rich

monomer in the synthesis of narrow band gap polymers. Polymers with tunable absorbances in the biologically relevant NIR-I and -II regions have been synthesized. As demonstrated in this work, one of the PDIz-based polymers shows a band gap as narrow as 0.7 eV, smaller than existing conjugated polymers with photothermal effects.[7] Such polymers have exhibited great photothermal conversion efficiencies that are effective for laser ablation of cancer cells, demonstrating their promise as photothermal therapeutic reagents. The PDIz system fills an increasingly important void in the small group of narrow band gap organic redox-active motifs. Its compatibility for incorporation into conjugated polymers opens the door to a wide range of band gap tunable materials.

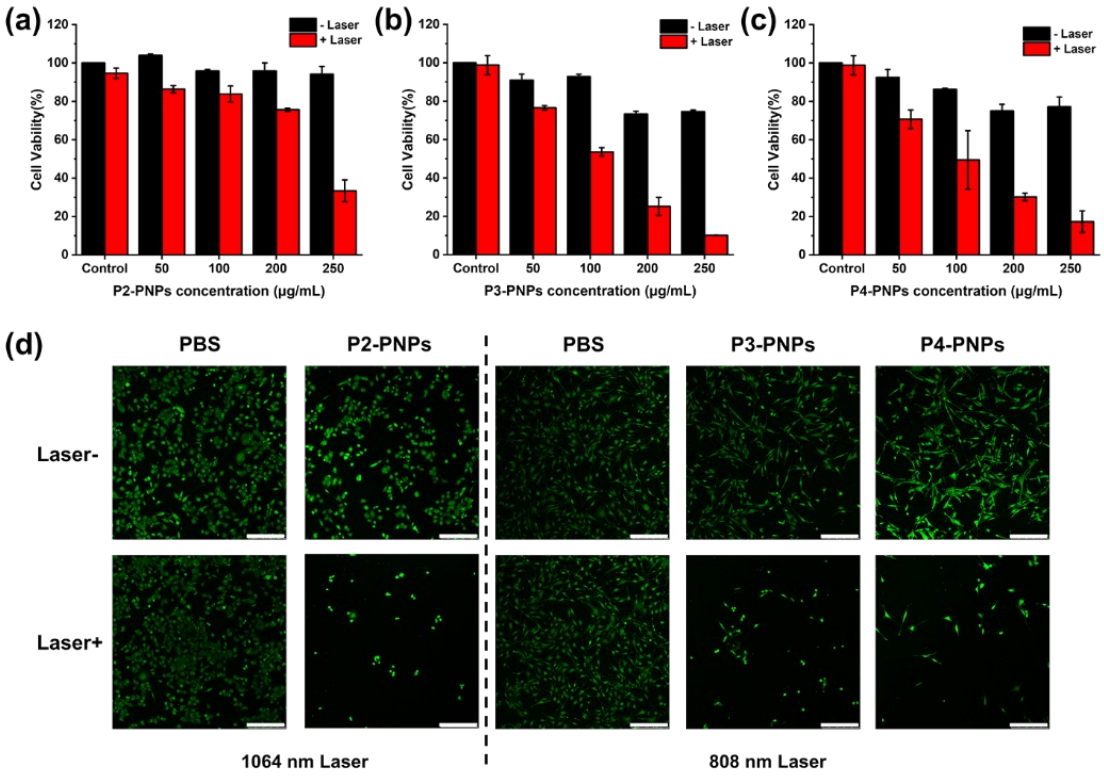

Figure 6. Cell viabilities of 4T1 cell lines incubated with different concentrations of (a) **P2**-PNPs, (b) **P3**-PNPs, and (c) **P4**-PNPs under 1064 nm or 808 nm irradiation at an output power of 1.5 W/cm^2 for 3 min. The quantified data were obtained from MTT (MTT: 3-(4,5-dimethylthiazol-2-yl)-2,5-diphenyltetrazolium bromide) assays. (d) Confocal laser scanning microscopy images of living cells incubated with PNPs and stained with calcein-AM after laser treatment. (scalebar: 250 μm for all images)

ASSOCIATED CONTENT

Supporting Information

The Supporting Information is available free of charge at http://pubs.acs.org. Details of synthetic procedures, solution NMR spectra, computational details, UV-vis, FT-IR and fluorescence spectra, X-ray crystallographic structures, spectroelectrochemical data, photothermal characterizations.

Accession Codes. CCDC 2165928, 2165929, 2165930, 2165931, 2165932 contain the supplementary crystallographic data for this paper. These data can be obtained free of charge via www.ccdc.cam.ac.uk/data_request/cif, or by emailing data_request@ccdc.cam.ac.uk, or by contacting The Cambridge Crystallographic Data Centre, 12 Union Road, Cambridge CB2 1EZ, UK; fax: +44 1223 336033.

AUTHOR INFORMATION

Corresponding Authors

Yi Liu–The Molecular Foundry, Lawrence Berkeley National Laboratory, Berkeley, California 94720, United States; Email: yliu@lbl.gov

Yongqin Lv– State Key Laboratory of Organic-Inorganic Composites, Beijing Key Laboratory of Bioprocess, Beijing University of Chemical Technology, Beijing, 100029, China; Email: lvyq@mail.buct.edu.cn

Authors

Christopher L. Anderson–The Molecular Foundry, Lawrence Berkeley National Laboratory, Berkeley, California 94720, United States; Email: chrislandsan@gmail.com

Tong Zhang– State Key Laboratory of Organic-Inorganic Composites, Beijing Key Laboratory of Bioprocess, Beijing University of Chemical Technology, Beijing, 100029, China; Email: 515921978@qq.com

Ziman Chen– State Key Laboratory of Organic-Inorganic Composites, Beijing Key Laboratory of Bioprocess, Beijing University of Chemical Technology, Beijing, 100029, China; Email: czm199209@126.com

Miao Qi- The Molecular Foundry, Lawrence Berkeley National Laboratory, Berkeley, California 94720, United States; Email: miaoqi@lbl.gov

Chongqing Yang- The Molecular Foundry, Lawrence Berkeley National Laboratory, Berkeley, California 94720, United States; Email: chongqing@lbl.gov

Simon J. Teat–Advanced Light Source, Lawrence Berkeley National Laboratory, Berkeley, California 94720, United States; Email: sjteat@lbl.gov

Nicholas S. Settineri–Department of Chemistry, University of California, Berkeley, California 94720, United States; Email: nsettine@berkeley.edu

Eric A. Dailing–The Molecular Foundry, Lawrence Berkeley National Laboratory, Berkeley, California 94720, United States; Email: edailing@lbl.gov

Andrés Garzón-Ruiz–Department of Physical Chemistry, Faculty of Pharmacy, Universidad de Castilla-La Mancha, Cronista Francisco Ballesteros Gómez, Albacete 02071, Spain; Email: Andres.Garzon@uclm.es

Amparo Navarro–Department of Physical and Analytical Chemistry, Faculty of Experimental Sciences, Universidad de Jaén, Campus Las Lagunillas, Jaén 23071, Spain; Email: anavarro@ujaen.es

Notes

The authors declare no competing financial interest.

Acknowledgements

This work was conducted at the Molecular Foundry, Lawrence Berkeley National Laboratory, and single crystal X-ray data was collected at BL11.3.1 and BL12.2.1 at Advanced Light Source, both being supported by the Office of Science, Office of Basic Energy Sciences, of the U.S. Department of Energy under Contract No. DE-AC02-05CH11231. Y.L. T.Z. and Z.C. acknowledge the financial support from the National Natural Science Foundation of China (Grant No. 22122801) and the Chinese Scholarship Council. The Centro de Servicios de Informática y Redes de Comunicaciones (CSIRC, Universidad de Granada), SCC (Universidad de Castilla-La Mancha) and Consejería de Transformación Económica, Industria, Conocimiento y Universidades/Junta de Andalucía (FQM-337) was instrumental in providing the computer time that made this work possible.

References

1. Scharber, M. C.; Sariciftci, N. S., Low Band Gap Conjugated Semiconducting Polymers. *Adv. Mater. Tech.* **2021,** *6* (4), 2000857.
2. Dou, L.; Liu, Y.; Hong, Z.; Li, G.; Yang, Y., Low-Bandgap Near-IR Conjugated Polymers/Molecules for Organic Electronics. *Chem. Rev.* **2015,** *115* (23), 12633-12665.
3. Vella, J. H.; Huang, L.; Eedugurala, N.; Mayer, K. S.; Ng, T. N.; Azoulay, J. D., Broadband infrared photodetection using a narrow bandgap conjugated polymer. *Sci. Adv.* **2021,** *7* (24), eabg2418.
4. Sun, H.; Lv, F.; Liu, L.; Gu, Q.; Wang, S., Conjugated Polymer Materials for Photothermal Therapy. *Adv. Ther.* **2018,** *1* (6), 1800057.
5. Wang, Y.; Meng, H.-M.; Song, G.; Li, Z.; Zhang, X.-B., Conjugated-Polymer-Based Nanomaterials for Photothermal Therapy. *ACS Appl. Poly. Mater.* **2020,** *2* (10), 4258-4272.
6. Li, L.; Han, X.; Wang, M.; Li, C.; Jia, T.; Zhao, X., Recent advances in the development of near-infrared organic photothermal agents. *Chem. Eng. J.* **2021,** *417*, 128844.
7. Lin, H.; Bai, H.; Yang, Z.; Shen, Q.; Li, M.; Huang, Y.; Lv, F.; Wang, S., Conjugated polymers for biomedical applications. *Chem. Commun.* **2022,** *58* (52), 7232-7244.
8. Lyu, Y.; Li, J.; Pu, K., Second Near-Infrared Absorbing Agents for Photoacoustic Imaging and Photothermal Therapy. *Small Methods* **2019,** *3* (11), 1900553.
9. Gao, D.; Hu, D.; Liu, X.; Zhang, X.; Yuan, Z.; Sheng, Z.; Zheng, H., Recent Advances in Conjugated Polymer Nanoparticles for NIR-II Imaging and Therapy. *ACS Appl. Poly. Mater.* **2020,** *2* (10), 4241-4257.
10. Men, X.; Yuan, Z., Polymer Dots for Precision Photothermal Therapy of Brain Tumors in the Second Near-Infrared Window: A Mini-Review. *ACS Appl. Poly. Mater.* **2020,** *2* (10), 4319-4330.
11. Müllen, K.; Pisula, W., Donor–Acceptor Polymers. *J. Am. Chem. Soc.* **2015,** *137* (30), 9503-9505.

12. Wang, Y.; Michinobu, T., Benzothiadiazole and its π-extended, heteroannulated derivatives: useful acceptor building blocks for high-performance donor–acceptor polymers in organic electronics. *J. Mater. Chem. C* **2016,** *4* (26), 6200-6214.
13. Qu, S.; Tian, H., Diketopyrrolopyrrole (DPP)-based materials for organic photovoltaics. *Chem. Commun.* **2012,** *48* (25), 3039-3051.
14. Nielsen, C. B.; Turbiez, M.; McCulloch, I., Recent Advances in the Development of Semiconducting DPP-Containing Polymers for Transistor Applications. *Adv. Mater.* **2013,** *25* (13), 1859-1880.
15. Kanimozhi, C.; Yaacobi-Gross, N.; Chou, K. W.; Amassian, A.; Anthopoulos, T. D.; Patil, S., Diketopyrrolopyrrole–Diketopyrrolopyrrole-Based Conjugated Copolymer for High-Mobility Organic Field-Effect Transistors. *J. Am. Chem. Soc.* **2012,** *134* (40), 16532-16535.
16. Bronstein, H.; Chen, Z.; Ashraf, R. S.; Zhang, W.; Du, J.; Durrant, J. R.; Shakya Tuladhar, P.; Song, K.; Watkins, S. E.; Geerts, Y.; Wienk, M. M.; Janssen, R. A. J.; Anthopoulos, T.; Sirringhaus, H.; Heeney, M.; McCulloch, I., Thieno[3,2-b]thiophene−Diketopyrrolopyrrole-Containing Polymers for High-Performance Organic Field-Effect Transistors and Organic Photovoltaic Devices. *J. Am. Chem. Soc.* **2011,** *133* (10), 3272-3275.
17. Li, W.; Roelofs, W. S. C.; Wienk, M. M.; Janssen, R. A. J., Enhancing the Photocurrent in Diketopyrrolopyrrole-Based Polymer Solar Cells via Energy Level Control. *J. Am. Chem. Soc.* **2012,** *134* (33), 13787-13795.
18. Yuen, J. D.; Fan, J.; Seifter, J.; Lim, B.; Hufschmid, R.; Heeger, A. J.; Wudl, F., High Performance Weak Donor–Acceptor Polymers in Thin Film Transistors: Effect of the Acceptor on Electronic Properties, Ambipolar Conductivity, Mobility, and Thermal Stability. *J. Am. Chem. Soc.* **2011,** *133* (51), 20799-20807.
19. Loser, S.; Bruns, C. J.; Miyauchi, H.; Ortiz, R. P.; Facchetti, A.; Stupp, S. I.; Marks, T. J., A Naphthodithiophene-Diketopyrrolopyrrole Donor Molecule for Efficient Solution-Processed Solar Cells. *J. Am. Chem. Soc.* **2011,** *133* (21), 8142-8145.
20. Zhan, X.; Facchetti, A.; Barlow, S.; Marks, T. J.; Ratner, M. A.; Wasielewski, M. R.; Marder, S. R., Rylene and Related Diimides for Organic Electronics. *Adv. Mater.* **2011,** *23* (2), 268-284.
21. Yan, H.; Chen, Z.; Zheng, Y.; Newman, C.; Quinn, J. R.; Dotz, F.; Kastler, M.; Facchetti, A., A high-mobility electron-transporting polymer for printed transistors. *Nature* **2009,** *457* (7230), 679-686.
22. Schmidt, R.; Ling, M. M.; Oh, J. H.; Winkler, M.; Könemann, M.; Bao, Z.; Würthner, F., Core-Fluorinated Perylene Bisimide Dyes: Air Stable n-Channel Organic Semiconductors for Thin Film Transistors with Exceptionally High On-to-Off Current Ratios. *Adv. Mater.* **2007,** *19* (21), 3692-3695.
23. Lv, A.; Puniredd, S. R.; Zhang, J.; Li, Z.; Zhu, H.; Jiang, W.; Dong, H.; He, Y.; Jiang, L.; Li, Y.; Pisula, W.; Meng, Q.; Hu, W.; Wang, Z., High Mobility, Air Stable, Organic Single Crystal Transistors of an n-Type Diperylene Bisimide. *Adv. Mater.* **2012,** *24* (19), 2626-2630.
24. Zhan, X.; Tan, Z. a.; Domercq, B.; An, Z.; Zhang, X.; Barlow, S.; Li, Y.; Zhu, D.; Kippelen, B.; Marder, S. R., A High-Mobility Electron-Transport Polymer with Broad Absorption and Its Use in Field-Effect Transistors and All-Polymer Solar Cells. *J. Am. Chem. Soc.* **2007,** *129* (23), 7246-7247.
25. Fukutomi, Y.; Nakano, M.; Hu, J.-Y.; Osaka, I.; Takimiya, K., Naphthodithiophenediimide (NDTI): Synthesis, Structure, and Applications. *J. Am. Chem. Soc.* **2013,** *135* (31), 11445-11448.

26. Zhao, J.; Wong, J. I.; Gao, J.; Li, G.; Xing, G.; Zhang, H.; Sum, T. C.; Yang, H. Y.; Zhao, Y.; Ake Kjelleberg, S. L.; Huang, W.; Joachim Loo, S. C.; Zhang, Q., Larger [small pi]-extended anti-/syn-aroylenediimidazole polyaromatic compounds: synthesis, physical properties, self-assembly, and quasi-linear conjugation effect. *RSC Adv.* **2014,** *4* (34), 17822-17831.
27. London, A. E.; Chen, H.; Sabuj, M. A.; Tropp, J.; Saghayezhian, M.; Eedugurala, N.; Zhang, B. A.; Liu, Y.; Gu, X.; Wong, B. M.; Rai, N.; Bowman, M. K.; Azoulay, J. D., A high-spin ground-state donor-acceptor conjugated polymer. *Sci. Adv.* **2019,** *5* (5), eaav2336.
28. Berens, H. R. V.; Müller, T. J. J., S,N-Heteropentacenes – Syntheses of Electron-Rich Anellated Pentacycles. *Org. Mater.* **2021,** *03* (02), 155-167.
29. Janiga, A.; Krzeszewski, M.; Gryko, D. T., Diindolo[2,3-b:2′,3′-f]pyrrolo[3,2-b]pyrroles as Electron-Rich, Ladder-Type Fluorophores: Synthesis and Optical Properties. *Chem. Asian J.* **2015,** *10* (1), 212-218.
30. Müller, M.; Ahrens, L.; Brosius, V.; Freudenberg, J.; Bunz, U. H. F., Unusual stabilization of larger acenes and heteroacenes. *J. Mater. Chem. C* **2019,** *7* (45), 14011-14034.
31. Sun, Z.; Wu, J., Higher Order Acenes and Fused Acenes with Near-infrared Absorption and Emission. *Aust. J. Chem.* **2011,** *64* (5), 519-528.
32. Okamoto, T.; Bao, Z., Synthesis of Solution-Soluble Pentacene-Containing Conjugated Copolymers. *J. Am. Chem. Soc.* **2007,** *129* (34), 10308-10309.
33. Kumarasamy, E.; Sanders, S. N.; Pun, A. B.; Vaselabadi, S. A.; Low, J. Z.; Sfeir, M. Y.; Steigerwald, M. L.; Stein, G. E.; Campos, L. M., Properties of Poly- and Oligopentacenes Synthesized from Modular Building Blocks. *Macromolecules* **2016,** *49* (4), 1279-1285.
34. Zhang, Z.; Zhang, Q., Recent progress in well-defined higher azaacenes (n ≥ 6): synthesis, molecular packing, and applications. *Mater. Chem. Front.* **2020,** *4* (12), 3419-3432.
35. Bunz, U. H. F.; Freudenberg, J., N-Heteroacenes and N-Heteroarenes as N-Nanocarbon Segments. *Acc. Chem. Res.* **2019,** *52* (6), 1575-1587.
36. Miao, Q., Ten Years of N-Heteropentacenes as Semiconductors for Organic Thin-Film Transistors. *Adv. Mater.* **2014,** *26* (31), 5541-5549.
37. Sadowski, B.; Klajn, J.; Gryko, D. T., Recent advances in the synthesis of indolizines and their π-expanded analogues. *Org. Biomol. Chem.* **2016,** *14* (33), 7804-7828.
38. Granger, D. B.; Mei, Y.; Thorley, K. J.; Parkin, S. R.; Jurchescu, O. D.; Anthony, J. E., Synthesis and Electrical Properties of Derivatives of 1,4-bis(trialkylsilylethynyl)benzo[2,3-b:5,6-b′]diindolizines. *Org. Lett.* **2016,** *18* (23), 6050-6053.
39. Anderson, C. L.; Dai, N.; Teat, S. J.; He, B.; Wang, S.; Liu, Y., Electronic Tuning of Mixed Quinoidal-Aromatic Conjugated Polyelectrolytes: Direct Ionic Substitution on Polymer Main-Chains. *Angew. Chem. Int. Ed.* **2019,** *58* (50), 17978-17985.
40. Liu, X.; He, B.; Anderson, C. L.; Kang, J.; Chen, T.; Chen, J.; Feng, S.; Zhang, L.; Kolaczkowski, M. A.; Teat, S. J., para-Azaquinodimethane: A Compact Quinodimethane Variant as an Ambient Stable Building Block for High-Performance Low Band Gap Polymers. *J. Am. Chem. Soc.* **2017,** *139* (24), 8355-8363.
41. Liu, X.; He, B.; Garzón-Ruiz, A.; Navarro, A.; Chen, T. L.; Kolaczkowski, M. A.; Feng, S.; Zhang, L.; Anderson, C. A.; Chen, J.; Liu, Y., Unraveling the Main Chain and Side Chain Effects on Thin Film Morphology and Charge Transport in Quinoidal Conjugated Polymers. *Adv. Funct. Mater.* **2018,** *28* (31), 1801874.
42. Anderson, C.; Liang, J.; Teat, S.; Garzon, A.; Nenon, D. P.; Navarro Rascón, A.; Liu, Y., A Highly Substituted Pyrazinophane Generated from a Quinoidal System via a Cascade Reaction. *Chem. Commun.* **2020,** *56*, 4472-4475.

43. Anderson, C. L.; Li, H.; Jones, C. G.; Teat, S. J.; Settineri, N. S.; Dailing, E. A.; Liang, J.; Mao, H.; Yang, C.; Klivansky, L. M.; Li, X.; Reimer, J. A.; Nelson, H. M.; Liu, Y., Solution-processable and functionalizable ultra-high molecular weight polymers via topochemical synthesis. *Nat. Commun.* **2021,** *12* (1), 6818.
44. Mondal, R.; Tönshoff, C.; Khon, D.; Neckers, D. C.; Bettinger, H. F., Synthesis, Stability, and Photochemistry of Pentacene, Hexacene, and Heptacene: A Matrix Isolation Study. *J. Am. Chem. Soc.* **2009,** *131* (40), 14281-14289.
45. Miao, Y.; Gu, C.; Yu, B.; Zhu, Y.; Zou, W.; Shen, Y.; Cong, H., Conjugated-Polymer-Based Nanoparticles with Efficient NIR-II Fluorescent, Photoacoustic and Photothermal Performance. *ChemBioChem* **2019,** *20* (21), 2793-2799.
46. Wang, S.; Riedinger, A.; Li, H.; Fu, C.; Liu, H.; Li, L.; Liu, T.; Tan, L.; Barthel, M. J.; Pugliese, G.; De Donato, F.; Scotto D'Abbusco, M.; Meng, X.; Manna, L.; Meng, H.; Pellegrino, T., Plasmonic Copper Sulfide Nanocrystals Exhibiting Near-Infrared Photothermal and Photodynamic Therapeutic Effects. *ACS Nano* **2015,** *9* (2), 1788-1800.
47. Hessel, C. M.; Pattani, V. P.; Rasch, M.; Panthani, M. G.; Koo, B.; Tunnell, J. W.; Korgel, B. A., Copper Selenide Nanocrystals for Photothermal Therapy. *Nano Lett.* **2011,** *11* (6), 2560-2566.
48. Lyu, Y.; Xie, C.; Chechetka, S. A.; Miyako, E.; Pu, K., Semiconducting Polymer Nanobioconjugates for Targeted Photothermal Activation of Neurons. *J. Am. Chem. Soc.* **2016,** *138* (29), 9049-9052.
49. Kim, J.; Lee, E.; Hong, Y.; Kim, B.; Ku, M.; Heo, D.; Choi, J.; Na, J.; You, J.; Haam, S.; Huh, Y.-M.; Suh, J.-S.; Kim, E.; Yang, J., Self-Doped Conjugated Polymeric Nanoassembly by Simplified Process for Optical Cancer Theragnosis. *Adv. Funct. Mater.* **2015,** *25* (15), 2260-2269.
50. Chen, P.; Ma, Y.; Zheng, Z.; Wu, C.; Wang, Y.; Liang, G., Facile syntheses of conjugated polymers for photothermal tumour therapy. *Nat. Commun.* **2019,** *10* (1), 1192.
51. Zhen, X.; Xie, C.; Pu, K., Temperature-Correlated Afterglow of a Semiconducting Polymer Nanococktail for Imaging-Guided Photothermal Therapy. *Angew. Chem. Int. Ed.* **2018,** *57* (15), 3938-3942.
52. Liu, Y.; Wang, H.; Li, S.; Chen, C.; Xu, L.; Huang, P.; Liu, F.; Su, Y.; Qi, M.; Yu, C.; Zhou, Y., In situ supramolecular polymerization-enhanced self-assembly of polymer vesicles for highly efficient photothermal therapy. *Nat. Commun.* **2020,** *11* (1), 1724.

Table of content graphic